rotating the whole laser-camera system mounted on a movable side of the robot; furthermore, cooperative 3-D laser scanning systems implemented by swarm robots or self-assembling modular robots will be investigated.

ACKNOWLEDGMENT

The authors would like to thank L. Ricotti and N. Funaro for fabricating prototypes of the Replicator robotic mechanical platform. The authors are also grateful to all the members involved in the Replicator project for their helpful suggestions and discussions.

REFERENCES

[1] T. Dutta and G. Fernie, "Utilization of ultrasound sensors for anti-Collision systems of powered wheelchairs," *IEEE Trans. Neural Syst. Rehabil. Eng.*, vol. 13, no. 1, pp. 24–32, Mar. 2005.
[2] F. Abrate, M. Indri, and B. Bona, "Monte carlo localization of minirovers with low-cost IR sensors," in *Proc. IEEE/ASME Int. Conf. Adv. Intell. Mechatron. (AIM)*, ETH Zurich, Switzerland, 2007, pp. 1–6.
[3] H. H. Cheng, B. D. Shaw, J. Palen, J. E. Larson, X. D. Hu, and K. Van, "A real-time laser-based detection system for measurement of delineations of moving vehicles," *IEEE/ASME Trans. Mechatronics*, vol. 6, no. 2, pp. 170–187, Jun. 2001.
[4] O. Duran, K. Althoefer, and L. D. Seneviratne, "Pipe inspection using a laser-based transducer and automated analysis Techniques," *IEEE/ASME Trans. Mechatronics*, vol. 8, no. 3, pp. 401–409, Sep. 2003.
[5] J. C. Zufferey and D. Floreano, "Toward 30-gram autonomous indoor aircraft: vision-based obstacle avoidance and altitude control," in *Proc. 2005 IEEE Int. Conf. Robot. Autom.*, Barcelona, Spain, 2005, pp. 2594–2599.
[6] H. Suzuki and M. Minami, "Visual servoing to catch fish using global/local GA search," *IEEE/ASME Trans. Mechatronics*, vol. 10, no. 3, pp. 352–357, Jun. 2005.
[7] E. C. Dean-Leon, V. Parra-Vega, and A. Espinosa-Romero, "Visual servoing for constrained planar robots subject to complex friction," *IEEE/ASME Trans. Mechatronics*, vol. 11, no. 4, pp. 389–400, Aug. 2006.
[8] REPLICATOR. [Online]. Available: http://www.replicators.eu/ (Accessed in 2010).
[9] SICK. [Online]. Available: http://www.sick.com/group/EN/ (Accessed in 2010).
[10] HOKUYO. [Online]. Available: http://www.hokuyo-aut.jp/ (Accessed in 2010).
[11] C. Ye and J. Borenstein, "A novel filter for terrain mapping with laser rangefinders," *IEEE Trans. Robot. Autom.*, vol. 20, no. 5, pp. 913–921, Oct. 2004.
[12] D. M. Cole and P. M. Newman, "Using laser range data for 3D SLAM in outdoor environments," in *Proc. IEEE Int. Conf. Robot. Autom.*, Orlando, FL, May 2006, pp. 1556–1563.
[13] V. Nguyen, A. Harati, A. Martinelli, R. Siegwart, and N. Tomatis, "Orthogonal slam: A step toward lightweight indoor autonomous navigation," in *Proc. IEEE/RSJ Int. Conf. Intell. Robots Syst.*, Beijing, China, 2006, pp. 5007–5012.
[14] S. Grzonka, G. Grisetti, and W. Burgard, "Towards a navigation system for autonomous indoor flying," in *Proc. IEEE Int. Conf. Robot. Autom.*, Kobe, Japan, 2009, pp. 2878–2883.
[15] E. Asadi and M. Bozorg, "A decentralized architecture for simultaneous localization and mapping," *IEEE/ASME Trans. Mechatronics*, vol. 14, no. 1, pp. 64–71, Feb. 2009.
[16] K. Yoshida and S. Hirose, "Laser triangulation range finder available under direct sunlight," in *Proc. Int. Conf. Robot. Autom.*, 1998, vol. 3, pp. 1702–1708.
[17] K. Konolige, J. Augenbraun, N. Donaldson, C. Fiebig, and P. Shah, "A low-cost laser distance sensor," in *Proc. Int. Conf. Robot. Autom.*, 2008, pp. 3002–3008.
[18] H. G. Nguyen and M. R. Blackburn, "A simple method for range finding via laser triangulation," Naval Command, Control and Ocean Surveillance Center, San Diego, CA, Tech. Rep., 1995.
[19] *Laser Safety: Safety of Laser Products—Part 1: Equipment Classification and Requirements*, 2nd ed., IEC, Geneva, Switzerland, 2007.
[20] *American National Standard for the Safe Use of Lasers*, ANSI Standard 2136.1-1993, p. 31, 32, 41, 42, 1993.
[21] M. Seelinger, "Development of a semi-autonomous multi-task robotics package using camera-space manipulation," Ph.D. dissertation, Univ. Notre Dame, Notre Dame, IN, 1996, pp. 51–61.
[22] B. Zhang, "Three-dimensional laser-assisted image analysis for robotic surface operation with camera-space manipulation," Ph.D. dissertation, Univ. Notre Dame, Notre Dame, IN, 2007, pp. 29–30.

Command State-Based Modifiable Walking Pattern Generation on an Inclined Plane in Pitch and Roll Directions for Humanoid Robots

Young-Dae Hong, Bum-Joo Lee, and Jong-Hwan Kim

***Abstract*—Previous research related to walking on an inclined plane for humanoid robots, including the 3-D linear inverted pendulum model (3D-LIPM) approach, were unable to modify walking period, step length, and walking direction independently without any additional step for adjusting the center of mass (CoM) motion. Moreover, the inclination along the pitch direction was only considered for walking. To solve these problems, a novel command state (CS)-based modifiable walking pattern generator for humanoid robots is proposed for modifiable walking on an inclined plane in both pitch and roll directions. The dynamic equation of the 3D-LIPM on the inclined plane in both pitch and roll directions is derived to obtain the CoM motion. Using the CoM motion, a method for modifiable walking pattern generation on the inclined plane is developed to follow a given CS composed of walking periods, step lengths, and walking directions for both legs. The effectiveness of the proposed walking pattern generator is demonstrated through both simulation and experiment for the small-sized humanoid robot, HanSaRam-IX (HSR-IX).**

***Index Terms*—3-D linear inverted pendulum model (3D-LIPM), command state (CS), humanoid robot, modifiable walking pattern generator (MWPG), walking on inclined plane, zero-moment point (ZMP).**

I. INTRODUCTION

Research on humanoid robots has made rapid progress such that various humanoid robots capable of stable walking with control algorithms have been developed [1]–[5]. A lot of control algorithms have been presented on the assumption that the plane is flat. However, in human environments, there exist not only flat but also inclined planes. Therefore, walking pattern generation on the inclined plane for humanoid robots is one of the key research issues.

As research on walking pattern generation on the inclined plane, Kajita and Tani proposed a linear inverted pendulum model (LIPM) to

Manuscript received July 9, 2010; revised September 2, 2010; accepted October 8, 2010. Date of publication December 3, 2010; date of current version May 11, 2011. Recommended by Technical Editor A. Menciassi. This work was supported by the Basic Science Research Program through the National Research Foundation of Korea funded by the Ministry of Education, Science and Technology under Grant 2010-0000831.

The authors are with the Department of Electrical Engineering, Korea Advanced Institute of Science and Technology (KAIST), Daejeon 305-701, Korea (e-mail: ydhong@rit.kaist.ac.kr; bjlee@rit.kaist.ac.kr; johkim@rit.kaist.ac.kr).

This paper has supplementary downloadable material available at http://ieeexplore.ieee.org, provided by the author. This material includes two videos with a total size of 2.81 MB. Contact johkim@rit.kaist.ac.kr for further questions about this work.

Digital Object Identifier 10.1109/TMECH.2010.2089530

control a biped walking on rugged terrain [6]. Zheng and Shen introduced an approach to measure the inclination of the plane using a foot system and then walk on the inclined plane by a simple modification of walking motion on a flat plane [7]. Shih and Chiou developed an approach to statically stable walking on the inclined plane maintaining the center of gravity of the robot within the convex hull of the supporting foot [8]. Chew *et al.* presented an approach to compute the hip height for dynamically stable walking on the inclined plane based on geometric consideration [9]. There was an approach to model a humanoid robot on the inclined plane as the 3D-LIPM and generate the trajectory of the center of mass (CoM) of the 3D-LIPM for walking on the inclined plane by the preview controller [10], [11]. Besides, there were some soft computing-based approaches to generate walking motion on the inclined plane by utilizing evolutionary algorithms [12], [13], neural network [14]–[16], fuzzy-logic, and their combinations [17].

The previous research on walking on the inclined plane, including 3D-LIPM approach, were unable to modify a walking pattern during the single support phase. Consequently, it was impossible to independently change walking pattern, i.e., walking period, step length, and walking direction on the inclined plane without any additional step for adjusting the CoM motion. Moreover, only the inclination along the pitch direction was considered for walking. In real environments, however, there exist inclined planes in roll as well as pitch directions.

To solve these problems, a proposed walking pattern generator is based on a modifiable walking pattern generator (MWPG), which has two closed form functions to allow zero-moment point (ZMP) variation in real time [18]. However, the MWPG can be only applied on the flat plane to modify walking period, step length and walking direction independently. Thus, a novel command state (CS)-based MWPG is proposed to be applied on the inclined plane in both pitch and roll directions. Initially, this paper derives the dynamic equation of the 3D-LIPM on the inclined plane in both pitch and roll directions to obtain the CoM motion with ZMP functions. Using the CoM motion, a method for modifiable walking pattern generation on the inclined plane is developed to follow a given CS composed of walking periods, step lengths, and walking directions for both legs. Once the CS is received, it is translated into the desired walking state (WS) defined by the position and velocity of the CoM in sagittal and lateral planes. Then, the control parameters of ZMP functions are solved to ensure the desired WS is attainable. The effectiveness of the proposed walking pattern generator is demonstrated through both simulation and experiment for the small-sized humanoid robot, HanSaRam-IX (HSR-IX), developed at the Robot Intelligence Technology (RIT) laboratory, Korea Advanced Institute of Science and Technology (KAIST).

This paper is organized as follows: Section II presents the dynamics of the 3D-LIPM on the inclined plane in both pitch and roll directions, and the CoM motion equations of the 3D-LIPM on the inclined plane are derived. In Section III, a method for modifiable walking pattern generation on the inclined plane is developed to follow a given CS. Section IV presents simulation and experimental results, and finally conclusions follow in Section V.

II. 3D-LIPM on Inclined Plane

A. Dynamics of 3D-LIPM on Inclined Plane

The walking of the humanoid robot is composed of single support phase and double support phase. In the single support phase, the primary dynamics of the humanoid robot on a flat plane can be modeled as a single inverted pendulum, which is called the 3D-LIPM [19]. It is assumed that the support leg is a weightless telescopic limb, and the mass is concentrated as a single point without vertical motion. Consequently, it is possible to decouple the equations of motion for sagittal and lateral planes. The 3D-LIPM can be extended to on the inclined plane in pitch and roll directions, as shown in Fig. 1. Using the extended model, the CoM trajectory for stable walking on the inclined plane can be obtained. The dynamic equation of the 3D-LIPM for the angular momentum taken around the contact point between the pendulum model and ground surface in the frame $\{R\}$, which lies on the inclined plane is written as follows:

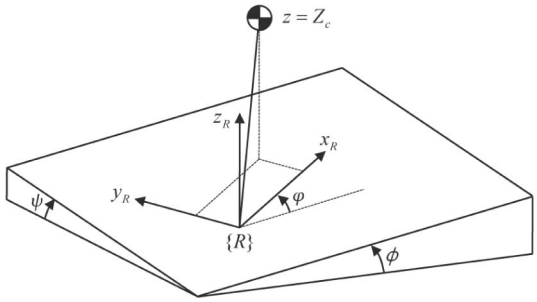

Fig. 1. 3D-LIPM on inclined plane in pitch and roll directions.

$$\mathbf{T}_{\rm gr} + \mathbf{r}_{\rm com} \times \mathbf{F}_{\rm gr} = \frac{d}{dt}(\mathbf{r}_{\rm com} \times \mathbf{L}) \tag{1}$$

where $\mathbf{T}_{\rm gr} = [T_x \;\; T_y \;\; T_z]^T$ represents the torque created by the ground reaction force, $\mathbf{r}_{\rm com} = [x \;\; y \;\; z]^T$ represents the vector from the contact point to the CoM, and $\mathbf{L}$ is the linear momentum of the CoM. Gravitational force $\mathbf{F}_{\rm gr}$ is given as follows:

$$\mathbf{F}_{\rm gr} = \begin{bmatrix} -mgS_\phi C_\varphi - mgS_\psi S_\varphi \\ mgS_\phi S_\varphi - mgS_\psi C_\varphi \\ -mgC_\phi C_\psi \end{bmatrix} \tag{2}$$

where m is the mass of the pendulum. S_θ and C_θ are defined as $\sin\theta$ and $\cos\theta$, respectively. ϕ and ψ represent the pitch and roll angles of the inclined plane, respectively. If ϕ is positive/negative, the plane is inclined upward/downward. Similarly, if ψ is positive/negative, the plane is inclined leftside/rightside. φ represents the yaw angle from the vertical direction of the inclined plane to the moving direction of the robot. Since the height of the CoM, z is constant Z_c, (1) can be rewritten as

$$\begin{bmatrix} \ddot{y} - \dfrac{gC_\phi C_\psi}{Z_c} y - gS_\phi S_\varphi + gS_\psi C_\varphi \\ \ddot{x} - \dfrac{gC_\phi C_\psi}{Z_c} x + gS_\phi C_\varphi + gS_\psi S_\varphi \end{bmatrix} = \begin{bmatrix} -\dfrac{T_x}{mZ_c} \\ \dfrac{T_y}{mZ_c} \end{bmatrix}. \tag{3}$$

The ZMP can be used to represent the sum of the torques caused by the ground reaction force as follows:

$$\mathbf{T}_{\rm gr} - \mathbf{r}_{\rm zmp} \times \mathbf{F}_{\rm gr} = [0 \quad 0 \quad M_z]^T \tag{4}$$

where $\mathbf{r}_{\rm zmp} = [x_{\rm zmp} \;\; y_{\rm zmp} 0]^T$ represents the ZMP, and M_z is the yaw moment. T_x and T_y are obtained from (4) and then the dynamic equation of the 3D-LIPM can be obtained by substituting them into (3) as follows:

$$\begin{bmatrix} \ddot{y} - \dfrac{gC_\phi C_\psi}{Z_c} y - gS_\phi S_\varphi + gS_\psi C_\varphi \\ \ddot{x} - \dfrac{gC_\phi C_\psi}{Z_c} x + gS_\phi C_\varphi + gS_\psi S_\varphi \end{bmatrix} = -\frac{gC_\phi C_\psi}{Z_c} \begin{bmatrix} y_{\rm zmp} \\ x_{\rm zmp} \end{bmatrix}. \tag{5}$$

The aforementioned equation provides the relationship between the ZMP and the CoM motion of the 3D-LIPM on the inclined plane in pitch and roll directions.

B. CoM Motion of 3D-LIPM on Inclined Plane

The solutions of (5), which mean the CoM motion of the 3D-LIPM on the inclined plane, are obtained by applying inverse Laplace transform as follows:
Sagittal motion:

$$\begin{bmatrix} x_f \\ v_f T_c \end{bmatrix} = \begin{bmatrix} Ch_T & Sh_T \\ Sh_T & Ch_T \end{bmatrix} \begin{bmatrix} x_i \\ v_i T_c \end{bmatrix} - \frac{1}{T_c} \begin{bmatrix} \int_0^T Sh_T \bar{p}(t)dt \\ \int_0^T Ch_T \bar{p}(t)dt \end{bmatrix} + \begin{bmatrix} -gT_c^2(S_\phi C_\varphi + S_\psi S_\varphi)(-1 + Ch_T) \\ -gT_c^2(S_\phi C_\varphi + S_\psi S_\varphi)Sh_T \end{bmatrix}.$$

Lateral motion:

$$\begin{bmatrix} y_f \\ w_f T_c \end{bmatrix} = \begin{bmatrix} Ch_T & Sh_T \\ Sh_T & Ch_T \end{bmatrix} \begin{bmatrix} y_i \\ w_i T_c \end{bmatrix} - \frac{1}{T_c} \begin{bmatrix} \int_0^T Sh_T \bar{q}(t)dt \\ \int_0^T Ch_T \bar{q}(t)dt \end{bmatrix} + \begin{bmatrix} -gT_c^2(-S_\phi S_\varphi + S_\psi C_\varphi)(-1 + Ch_T) \\ -gT_c^2(-S_\phi S_\varphi + S_\psi C_\varphi)Sh_T \end{bmatrix} \quad (6)$$

with

$$T_c = \sqrt{\frac{Z_c}{gC_\phi C_\psi}}$$

where $(x_i, v_i)/(x_f, v_f)$ and $(y_i, w_i)/(y_f, w_f)$ represent initial/final position and velocity of the CoM in sagittal and lateral planes, respectively. Sh_t and Ch_t are defined as $\sinh(t/T_c)$ and $\cosh(t/T_c)$, respectively, T is the remaining single support time, and $p(t)$ and $q(t)$ are ZMP functions for sagittal and lateral motions, respectively, where $\overline{p}(t) = p(T - t)$ and $\overline{q}(t) = q(T - t)$.

The first terms on the right-hand side of (6) indicate homogeneous solutions of (5). The second terms represent additional states (particular solutions) that allow more extensive and unrestricted motions by varying ZMP trajectories with $p(t)$ and $q(t)$. In the conventional 3D-LIPM approach, the particular solutions have not been considered, assuming that the ZMP is fixed at the contact point. Consequently, the dynamics for the CoM motion of the 3D-LIPM is predetermined and unmodifiable throughout the single support phase. Thus, it is impossible to modify walking pattern, i.e. walking period, step length, and walking direction independently in the conventional 3D-LIPM. When the step length is changed, the walking period has to be also changed because they are dependent. The last terms perform shifting the CoM trajectory of the 3D-LIPM for walking on the inclined plane according to the pitch and roll angles of the plane and the yaw angle of the robot (ϕ, ψ, and φ).

In order to vary the ZMP trajectory effectively, suitable ZMP functions $p(t)$ and $q(t)$ should be provided. Among infinitely many candidate functions, in terms of implementation, the constant function and the step function are selected for $p(t)$ and $q(t)$, respectively, as shown in Fig. 2 [18]. In the figure, P and Q are the magnitudes of constant and step functions, respectively, and $T_{\rm sw}$ is the switching time of step function.

To formulate the state of the single inverted pendulum, the following WS is defined with the position and velocity of the CoM in sagittal and lateral planes [18].

Definition 1: Walking state is defined as

$$\mathbf{x} = [\, x \quad T_c v \,]^T \text{ for sagittal motion}$$
$$\mathbf{y} = [\, y \quad T_c w \,]^T \text{ for lateral motion.}$$

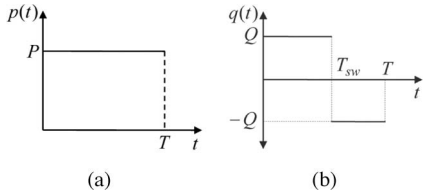

Fig. 2. ZMP functions. (a) Constant function for sagittal motion. (b) Step function for lateral motion.

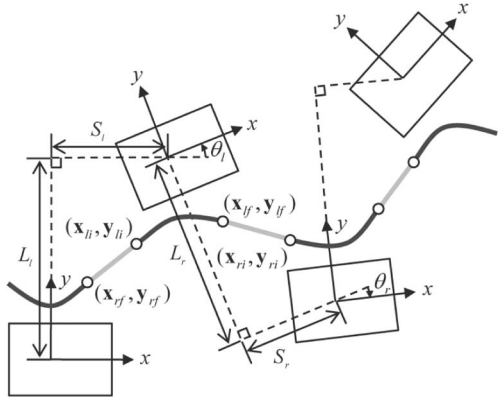

Fig. 3. Walking configuration in steady state. The rectangles represent the foot boundaries and the thick and thin lines represent the CoM trajectories in single support phase and double support phase, respectively. The small circles represent the initial/final CoM positions for left/right support phase.

Note that the WS is represented as a two dimensional vector in each plane and the velocity terms are multiplied with T_c.

III. Method for Modifiable Walking Pattern Generation on Inclined Plane

A. Command State

As a minimal navigational command set to generate a walking pattern, CS is defined with single and double support times, step lengths, and walking directions for both legs [18].

Definition 2: Command state is defined as

$$\mathbf{c} \equiv [T_{sl} \;\; T_{dl} \;\; S_l \;\; L_l \;\; \theta_l \;\; T_{sr} \;\; T_{dr} \;\; S_r \;\; L_r \;\; \theta_r]$$

where

- $T_{sl/r}$ single support time during left/right support phase;
- $T_{dl/r}$ double support time from left/right support phase to right/left support;
- $S_{l/r}$ sagittal step length of left/right leg;
- $L_{l/r}$ lateral step length of left/right leg;
- $\theta_{l/r}$ direction of left/right leg.

B. Translating CS Into Desired WS

Since walking is a repetitive motion, its behavior can be described by identifying the WSs at particular points in the motion. When the robot follows a given CS, it is assumed that its state is in steady state and ZMP variation is not utilized. These assumptions correspond directly to a walking pattern that represents steady-state motion for the 3D-LIPM in which the particular solutions of (6) are zero. In this situation, the WS at the end of each single support phase is identical. This state is considered as a desired WS.

To translate the CS into the desired WS, it is enough to observe only one period of the walking configuration in steady state, as shown in Fig. 3. According to the CS, sagittal and lateral motions are generally

nonsymmetrical for both left and right legs with different single and double support times, step lengths, and walking directions. Since the robot's state is in steady state without ZMP variation, the walking configuration can be fully described by initial or final WS for both left and right leg support phases. In terms of implementation, the CoM is controlled to travel with constant velocity during double support phase for a specific time $T_{dl/r}$ for double support from left/right to right/left movement.

Notation 1: In the derivation, the following notations are used:

$\mathbf{x}_{li}$ initial WS of sagittal motion for left support phase;
$\mathbf{x}_{lf}$ final WS of sagittal motion for left support phase;
$\mathbf{x}_{ri}$ initial WS of sagittal motion for right support phase;
$\mathbf{x}_{rf}$ final WS of sagittal motion for right support phase.

Note that the WSs $\mathbf{y}_{li}$, $\mathbf{y}_{lf}$, $\mathbf{y}_{ri}$, and $\mathbf{y}_{rf}$ are defined in a similar manner to the case for sagittal motion. Each WS is defined with respect to the local coordinate frame attached on its support leg.

From the equations of motion, (6) with $\overline{p}(t) = 0$ and $\overline{q}(t) = 0$, the following two state equations, which represent left- and right-single support phases, respectively, are obtained during single support phase:

$$\begin{aligned} Z_{lf} &= A_{T_{sl}} Z_{li} + E_l \\ Z_{rf} &= A_{T_{sr}} Z_{ri} + E_r \end{aligned} \tag{7}$$

where

$$Z = [\,\mathbf{x} \quad \mathbf{y}\,] \quad A_t = \begin{bmatrix} Ch_t & Sh_t \\ Sh_t & Ch_t \end{bmatrix} \quad E_{l/r} = [\,E_{sl/r} \quad E_{ll/r}\,]$$

$$E_{sl/r} = \begin{bmatrix} -gT_c^2(S_\phi C_\varphi + S_\psi S_\varphi)(-1 + Ch_{T_{sl/r}}) \\ -gT_c^2(S_\phi C_\varphi + S_\psi S_\varphi) Sh_{T_{sl/r}} \end{bmatrix}$$

$$E_{ll/r} = \begin{bmatrix} -gT_c^2(-S_\phi S_\varphi + S_\psi C_\varphi)(-1 + Ch_{T_{sl/r}}) \\ -gT_c^2(-S_\phi S_\varphi + S_\psi C_\varphi) Sh_{T_{sl/r}} \end{bmatrix}.$$

After double support time, the final WSs of single support phase become the initial WSs of the next support phase as follows:

$$\begin{aligned} Z_{li} &= (U_{T_{dr}} Z_{rf} - D_l) R_{\theta_r} \\ Z_{ri} &= (U_{T_{dl}} Z_{lf} - D_r) R_{\theta_l} \end{aligned} \tag{8}$$

where

$$R_\theta = \begin{bmatrix} C_\theta & S_\theta \\ -S_\theta & C_\theta \end{bmatrix} \quad U_t = \begin{bmatrix} 1 & \dfrac{t}{T_C} \\ 0 & 1 \end{bmatrix} \quad D_{l/r} = \begin{bmatrix} S_{l/r} & L_{l/r} \\ 0 & 0 \end{bmatrix}.$$

By substituting (8) into (7), relationships between final WSs are derived as follows:

$$\begin{aligned} Z_{lf} &= A_{T_{sl}} U_{T_{dr}} Z_{rf} R_{\theta_r} - A_{T_{sl}} D_l R_{\theta_r} + E_l \\ Z_{rf} &= A_{T_{sr}} U_{T_{dl}} Z_{lf} R_{\theta_l} - A_{T_{sr}} D_r R_{\theta_l} + E_r. \end{aligned} \tag{9}$$

By using Kronecker product [21], (9) can be transformed to the following vectorial matrix equations:

$$\begin{aligned} \boldsymbol{\zeta}_{lf} &= A_r^* \boldsymbol{\zeta}_{rf} - \mathbf{b}_r^* + \mathbf{e}_l \\ \boldsymbol{\zeta}_{rf} &= A_l^* \boldsymbol{\zeta}_{lf} - \mathbf{b}_l^* + \mathbf{e}_r \end{aligned} \tag{10}$$

with

$$\begin{aligned} A_r^* &= R_{\theta_r}^T \otimes (A_{T_{sl}} U_{T_{dr}}), \quad A_l^* = R_{\theta_l}^T \otimes (A_{T_{sr}} U_{T_{dl}}) \\ \mathbf{b}_r^* &= (R_{\theta_r}^T \otimes A_{T_{sl}}) \mathbf{d}_l, \quad \mathbf{b}_l^* = (R_{\theta_l}^T \otimes A_{T_{sr}}) \mathbf{d}_r \end{aligned}$$

where $\otimes$ represents the Kronecker product. If $A \in \Re^{m \times n}$ and $B \in \Re^{p \times q}$, then their Kronecker product $A \otimes B$ is the $m \times n$ block matrix whose (i, j) block is the $p \times q$ matrix $a_{ij} B$ as follows:

$$A \otimes B = \begin{bmatrix} a_{11} B & \cdots & a_{1n} B \\ \vdots & \ddots & \vdots \\ a_{m1} B & \cdots & a_{mn} B \end{bmatrix}. \tag{11}$$

The Kronecker product can be used to get a convenient representation for some matrix equations. For instance, the equation $AXB = C$, for given matrices A, B, and C, and the unknown matrix X, can be rewritten as follows:

$$(B^T \otimes A)\mathrm{vec}(X) = \mathrm{vec}(AXB) = \mathrm{vec}(C) \tag{12}$$

where $\mathrm{vec}(X)$ denotes the vectorization of the matrix X formed by stacking the columns of X into a single column vector. $\boldsymbol{\zeta}_{l/rf}$, $\mathbf{d}_{l/r}$, and $\mathbf{e}_{l/r}$ are $\mathrm{vec}(Z_{l/rf})$, $\mathrm{vec}(D_{l/r})$, and $\mathrm{vec}(E_{l/r})$, respectively. Finally, (10) gives

$$\begin{aligned} \boldsymbol{\zeta}_{lf} &= (A_r^* A_l^* - \mathbf{I})^{-1} (A_r^* \mathbf{b}_l^* - A_r^* \mathbf{e}_r + \mathbf{b}_r^* - \mathbf{e}_l) \\ \boldsymbol{\zeta}_{rf} &= (A_l^* A_r^* - \mathbf{I})^{-1} (A_l^* \mathbf{b}_r^* - A_l^* \mathbf{e}_l + \mathbf{b}_l^* - \mathbf{e}_r) \end{aligned} \tag{13}$$

where $\mathbf{I}$ is the identity matrix. This represents the mapping relationship between the CS and the desired WS. Once the CS is received, it is translated into the desired WS form. The desired WS while in single support phase becomes $\boldsymbol{\zeta}_{lf}$ or $\boldsymbol{\zeta}_{rf}$ for the left or right support phase, respectively. The information about the CS lies in the matrices $A_{l/r}^*$, $\mathbf{b}_{l/r}^*$, and $\mathbf{e}_{l/r}$.

C. Control Parameters

The control parameters T, P, T_{sw}, and Q, which characterize the ZMP functions (see Fig. 2), should be solved to ensure that the desired WS is attainable. The values of the ZMP functions $p(t)$ and $q(t)$ are zero when the CS does not change. ZMP variation occurs whenever the CS changes. This corresponds to the particular solutions that accelerate or decelerate the CoM until the current WS matches the desired WS. T represents the remaining time in the single support for the current step to achieve the desired WS. Therefore, it is generally not identical to the commanded single support time $T_{sl/r}$ of the given CS until the end of the current single support phase when the desired WS is achieved.

1) Sagittal Motion: From (6) for the sagittal motion with $t = T$ and $p(t) = P$, control parameters T and P are calculated as follows:

$$\begin{aligned} T &= T_c \ln\left(\frac{(v_d + v_i)T_c + (x_d - x_i)}{(v_d + v_i)T_c - (x_d - x_i)}\right) \\ P &= \frac{(x_d^2 - x_i^2) - (v_d^2 - v_i^2)T_c^2}{2(x_d - x_i)} - gT_c^2(S_\phi C_\varphi + S_\psi S_\varphi) \end{aligned} \tag{14}$$

where $[x_d \;\; T_c v_d]^T$ represents the desired WS.

2) Lateral Motion: The homogeneous part of (6) for the lateral motion is determined by the initial WS and the precalculated T from the sagittal motion. Therefore, it is only necessary to consider the particular solution. Letting

$$q(t) = \begin{cases} Q, & \text{if } 0 \le t < T_{\mathrm{sw}} \\ -Q, & \text{if } T_{\mathrm{sw}} \le t \le T \end{cases}$$

the particular solution of (6) for the lateral motion is derived as follows:

$$\begin{bmatrix} y_p \\ T_c w_p \end{bmatrix} = \begin{bmatrix} 2Ch_{T-T_{\mathrm{sw}}} - (1 + Ch_T) \\ 2Sh_{T-T_{\mathrm{sw}}} - Sh_T \end{bmatrix} Q. \tag{15}$$

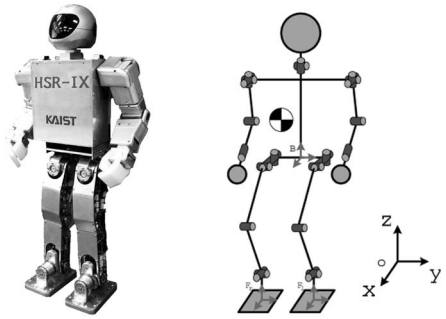

(a) (b)

Fig. 4. Humanoid robot. (a) HanSaRam-IX. (b) Configuration.

From (15), $T_{\rm sw}$ and Q are calculated as follows:

$$T_{\rm sw} = T - T_c \ln(h), \quad 0 \le T_{\rm sw} \le T$$
$$Q = \frac{y_p}{(h + h^{-1}) - (1 + Ch_T)} \tag{16}$$

where

$$h = \begin{cases} \dfrac{\gamma + \sqrt{\gamma^2 + 4\alpha\beta}}{2\alpha}, & \text{if } \delta < 0 \\ 1, & \text{if } \delta = 0 \\ \dfrac{\gamma - \sqrt{\gamma^2 + 4\alpha\beta}}{2\alpha}, & \text{if } \delta > 0 \end{cases}$$
$$\alpha = y_p - T_c w_p \qquad \beta = y_p + T_c w_p$$
$$\gamma = y_p S h_T - T_c w_p (1 + Ch_T)$$
$$\delta = y_p S h_T + T_c w_p (1 - Ch_T).$$

From (14) and (16), the control parameters are directly calculated from the current and the desired WSs.

D. Overall Procedure of Proposed Algorithm

In this paper, it is assumed that the pitch and roll plane angles are measurable. For each sample time, the proposed algorithm receives a CS and translates it into a desired WS using (13). Next, control parameters T, P, $T_{\rm sw}$, and Q for the ZMP functions are calculated to achieve the desired WS using (14) and (16). Then, the WS is calculated using (6). Subsequently, the CoM motion of the 3D-LIPM is updated. Trajectories of every leg joint are obtained by inverse kinematics.

IV. Simulation and Experiment

The proposed algorithm was implemented on the small-sized humanoid robot, HanSaRam-IX (HSR-IX) (see Fig. 4). HSR-IX has been in continual development and research by the RIT Laboratory at KAIST [3]. Its height and weight are 52.8 cm and 5.5 kg, respectively. It has 26 DOF, which consists of 12 dc motors with harmonic drives in the lower body and 16 RC servo motors in the upper body. The on-board Pentium-III compatible PC, running RT-Linux, calculates the proposed algorithm every 5 ms in real time. To measure ground reaction forces on the feet and the real ZMP trajectory while walking, four force sensing resisters are equipped on the sole of each foot.

TABLE I
CS list (time units, length units, and angle units were given in seconds, centimeters, and degrees, respectively.)

	T_{sl}	T_{dl}	S_l	L_l	θ_l	T_{sr}	T_{dr}	S_r	L_r	θ_r
Initial CS	0.8	0.4	4.0	6.0	0.0	0.8	0.4	4.0	−6.0	0.0
After 2^{nd} step	0.8	0.4	1.0	6.0	0.0	0.8	0.4	1.0	−10.0	0.0
After 3^{rd} step	0.8	0.4	4.0	6.0	0.0	0.8	0.4	4.0	−6.0	0.0
After 5^{th} step	0.8	0.4	2.0	9.0	0.0	0.8	0.4	2.0	−6.0	0.0
After 6^{th} step	0.8	0.4	4.0	6.0	0.0	0.8	0.4	4.0	−6.0	0.0
After 9^{th} step	0.8	0.4	2.0	9.0	0.0	0.8	0.4	2.0	−6.0	0.0
After 10^{th} step	0.8	0.4	4.0	6.0	0.0	0.8	0.4	4.0	−6.0	−10.0
After 11^{th} step	0.8	0.4	4.0	6.0	0.0	0.8	0.4	4.0	−6.0	0.0
After 12^{th} step	0.8	0.4	0.0	6.0	0.0	0.8	0.4	0.0	−6.0	0.0

A. Simulation Result

The simulation was carried out using the simulation model of HSR-IX modeled by Webot, which is the 3-D robotics simulation software and enables users to conduct the physical and dynamical simulation [20]. In the simulation environment, the plane was inclined upward and left side simultaneously and allowable pitch and roll plane angles ϕ and ψ were from -20.0° to 20.0° and from -8.0° to 8.0°, respectively, for the robot to walk straight while maintaining stability. In this simulation, ϕ and ψ were set as 15.0° and 5.0°, respectively. The CS list for the simulation is shown in Table I, in which sagittal and lateral step lengths and walking direction were independently changed while maintaining the same walking period at each footstep.

Fig. 5 shows the generated walking pattern, CoM, and ZMP trajectories in the simulation (Video 1). As shown in the figure, the robot started to walk from the position $[0.0 \;\; 0.0]^T$ and followed the given CS list successfully. The CoM trajectory, which was shifted forward and left simultaneously compared to that on the flat plane, was generated. Namely, by means of generating the shifted CoM trajectory, the robot was able to walk stably on the inclined plane because the ZMP was within the foot boundary. It can be shown that the ZMP trajectories in x-axis and y-axis followed the foot trajectories with a small variation. The small variation of ZMP trajectories was mainly caused by the dynamic difference between the robot and the 3D-LIPM. However, the ZMP trajectories were within the upper and lower boundaries of foot trajectories. Accordingly, the robot was able to walk stably on the inclined plane in both pitch and roll directions.

B. Experiment Result

The experiment was carried out using the real small-sized humanoid robot, HSR-IX. In the experiment environment, the plane was inclined upward and left side simultaneously and allowable pitch and roll plane angles ϕ and ψ were from -12.0° to 12.0° and from -6.0° to 6.0°, respectively, for the robot to walk straight while maintaining stability. In this experiment, ϕ and ψ were set as 8.0° and 4.0°, respectively. The difference between pitch and roll plane angles in simulation and experiment is because there were measurement noise, offset, and unmodeled errors in the real robot, including joint compliance and the slip between the robot and the plane, which led to the larger variation of the ZMP trajectories. The CS list for the experiment was the same as that for the simulation except for rotation motion. The rotation motion was not considered because of the slip between the robot and the plane. When the robot changed the walking direction on the inclined plane, the slip occurred. Then the robot fell down since the ZMP variation more increased.

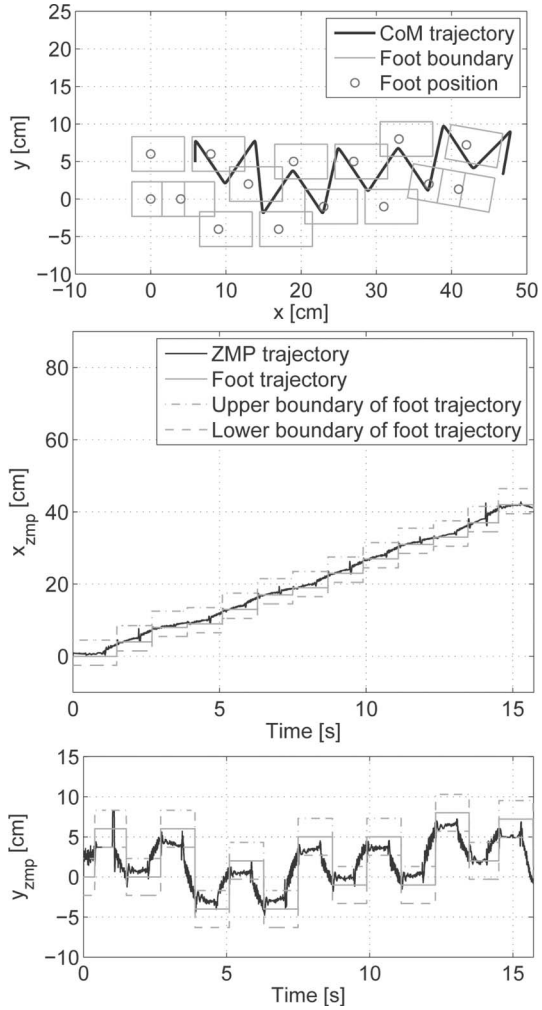

Fig. 5. Generated walking pattern, CoM, and ZMP trajectories when the plane was inclined upward and left side simultaneously in the simulation ($\phi = 15.0^\circ$ and $\psi = 5.0^\circ$).

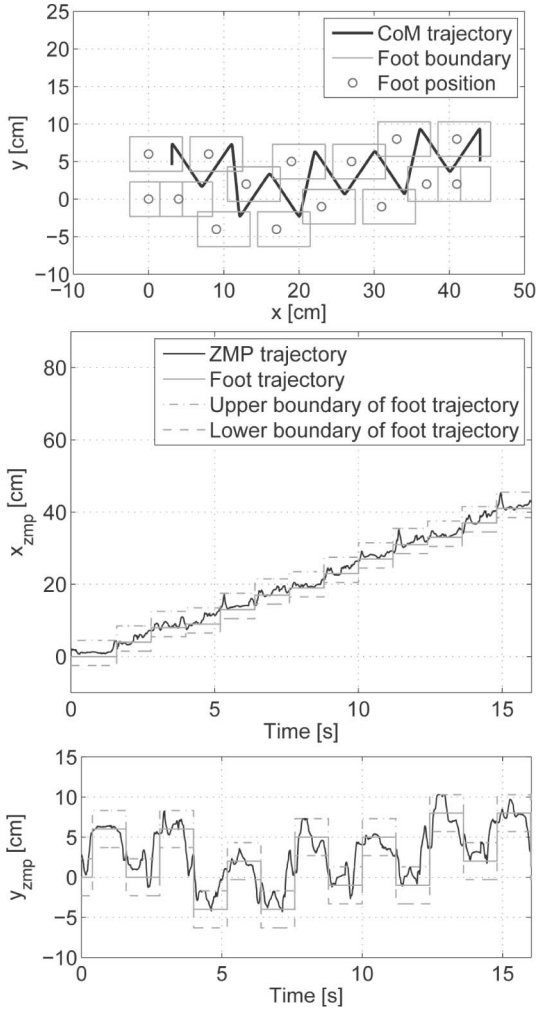

Fig. 6. Generated walking pattern, CoM, and ZMP trajectories when the plane was inclined upward and left side simultaneously in the experiment ($\phi = 8.0^\circ$ and $\psi = 4.0^\circ$).

Fig. 6 shows the generated walking pattern, CoM, and ZMP trajectories in the experiment (Video 2). As shown in the figure, the robot followed the given CS list successfully and the ZMP trajectories in x-axis and y-axis followed the foot trajectories with a little variation. Compared with the simulation result, the variation of the ZMP trajectories was larger because of the unmodeled errors in the real robot mentioned earlier. However, the ZMP trajectories were within the upper and lower boundaries of foot trajectories. Accordingly, the robot was able to walk stably on the inclined plane in both pitch and roll directions.

V. Conclusion

In this paper, the CS-based MWPG on the inclined plane in pitch and roll directions for humanoid robots was proposed and verified through both simulation and experiment for the small-sized humanoid robot, HSR-IX. The proposed walking pattern generator independently changed walking period, step length, and walking direction on the inclined plane without any extra step for adjusting the CoM motion. To obtain the CoM motion of the 3D-LIPM with ZMP functions, the dynamic equation of the 3D-LIPM on the inclined plane in both pitch and roll directions was derived. Moreover, to follow the given CS, the method for modifiable walking pattern generation on the inclined plane was developed. Consequently, by using the proposed walking pattern generator, the humanoid robot could walk stably on the inclined plane in both pitch and roll directions following the commanded CS list in which sagittal and lateral step lengths and walking direction were independently changed while maintaining the same walking period at each footstep.

In this paper, the robot can vary the WS by varying the ZMP trajectory. However, this does not mean that the robot has the ability to change its WS to any desired WS. If the ZMP exceeds the support polygon, the robot is unable to walk stably. To solve this problem, allowable ZMP variation region has to be defined, which is within the support polygon. Then when the ZMP exceeds the region, the desired WS has to be substituted to the WS as close as possible to the desired one, for which the ZMP is within the support polygon. To satisfy the substituted WS, the CS has to be changed. Also, for changing the walking direction of HSR-IX on the inclined plane, it needs a more complicated controller to deal with the slip between the robot and the plane and to minimize the ZMP variation. These remain as further works.

References

[1] Y. Sakagami, R. Watanabe, C. Aoyama, S. Matsunaga, N. Higaki, and K. Fujimura, "The intelligent ASIMO: System overview and integration," in *Proc. IEEE/RSJ Int. Conf. Intell. Robot. Syst.*, 2002, pp. 2478–2483.

[2] E. S. Neo, K. Yokoi, S. Kajita, F. Kanehiro, and K. Tanie, "A switching command-based whole-body operation method for humanoid robots," *IEEE/ASME Trans. Mechtronics*, vol. 10, no. 5, pp. 546–559, Oct. 2005.

[3] J.-K. Yoo, B.-J. Lee, and J.-H. Kim, "Recent progress and development of the humanoid robot HanSaRam," *Robot. Auton. Syst.*, vol. 57, no. 10, pp. 973–981, 2009.

[4] T. Aoyama, Y. Hasegawa, K. Sekiyama, and T. Fukuda, "Stabilizing and direction control of efficient 3-D biped walking based on PDAC," *IEEE/ASME Trans. Mechtronics*, vol. 14, no. 6, pp. 712–718, Dec. 2009.

[5] K. Harada, S. Hattori, H. Hirukawa, M. Morisawa, S. Kajita, and E. Yoshida, "Two-stage time-parametrized gait planning for humanoid robots," *IEEE/ASME Trans. Mechtronics*, vol. 15, no. 5, pp. 694–703, Oct. 2010.

[6] S. Kajita and K. Tani, "Study of dynamic biped locomotion on rugged terrain—Derivation and application of the linear inverted pendulum mode," in *Proc. IEEE Int. Conf. Robot. Autom.*, 1991, pp. 1405–1411.

[7] Y. F. Zheng and J. Shen, "Gait synthesis for the SD-2 biped robot to climb sloping surface," *IEEE Trans. Robot. Autom.*, vol. 6, no. 1, pp. 86–96, Feb. 1990.

[8] C.-L. Shih and C.-J. Chiou, "The motion control of a statically stable biped robot on an uneven floor," *IEEE Trans. Syst. Man, Cybern. B, Cybern.*, vol. 28, no. 2, pp. 244–249, Apr. 1998.

[9] C.-M. Chew, J. Pratt, and G. Pratt, "Blind walking of a planar bipedal robot on sloped terrain," in *Proc. IEEE Int. Conf. Robot. Autom.*, 1999, vol. 1, pp. 381–386.

[10] S. Kajita, F. Kanehiro, K. Kaneko, K. Fujiwara, K. Harada, K. Yokoi, and H. Hirukawa, "Biped walking pattern generation by using preview control of zero-moment point," in *Proc. IEEE Int. Conf. Robot. Autom.*, 2003, vol. 2, pp. 1620–1626.

[11] W. Huang, C.-M. Chew, Y. Zheng, and G.-S. Hong, "Pattern generation for bipedal walking on slopes and stairs," in *Proc. IEEE-RAS Int. Conf. Humanoid Robots*, 2008, pp. 205–210.

[12] Y. Hasegawa, T. Arakawa, and T. Fukuda, "Trajectory generation for biped locomotion robot," *Mechatronics*, vol. 10, pp. 67–89, 2000.

[13] L. Yang, C.-M. Chew, T. Zielinska, and A.-N. Poo, "A uniform biped gait generator with offline optimization and online adjustable parameters," *Robotica*, vol. 25, pp. 549–565, 2007.

[14] G. Taga, Y. Yamaguehi, and H. Shimizu, "Self-organized control of bipedal locomotion by neural oscillators in unpredictable environment," *Biol. Cybern.*, vol. 65, no. 3, pp. 147–159, 1991.

[15] A. W. Salatian, K. Y. Yi, and Y. F. Zheng, "Reinforcement learning for a biped robot to climb sloping surfaces," *J. Robot. Syst.*, vol. 14, no. 4, pp. 283–296, 1997.

[16] S. Aoi and K. Tsuchiya, "Locomotion control of a biped robot using nonlinear oscillators," *Auton. Robots*, vol. 19, no. 3, pp. 219–232, 2005.

[17] P. R. Vundavilli and D. K. Pratihar, "Soft computing-based gait planners for a dynamically balanced biped robot negotiating sloping surfaces," *Appl. Soft Comput. J.*, vol. 9, no. 1, pp. 191–208, 2009.

[18] B.-J. Lee, D. Stonier, Y.-D. Kim, J.-K. Yoo, and J.-H. Kim, "Modifiable walking pattern of a humanoid robot by using allowable ZMP variation," *IEEE Trans. Robot.*, vol. 24, no. 4, pp. 917–925, Aug. 2008.

[19] S. Kajita, F. Kanehiro, K. Kaneko, K. Fujiwara, K. Yokoi, and H. Hirukawa, "A realtime pattern generator for biped walking," in *Proc. IEEE Int. Conf. Robot. Autom.*, 2002, vol. 1, pp. 31–37.

[20] O. Michel, "Cyberbotics Ltd. WebotsTM: Professional mobile robot simulation," *Int. J. Adv. Robot. Syst.*, vol. 1, no. 1, pp. 39–42, 2004.

[21] H. V. Henderson and S. R. Searle, "The vec-permutation matrix, the vec operator and kronecker products: A review," *Linear Multilinear Algebra*, vol. 9, no. 4, pp. 271–288, 1981.